Resonant behavior of trapped Brownian particles in an oscillatory shear flow

Hanno Kählert and Hartmut Löwen[*]

Heinrich-Heine-Universität Düsseldorf, Institut für Theoretische Physik II: Weiche Materie,
Universitätsstraße 1, 40225 Düsseldorf, Germany

The response of harmonically trapped Brownian particles to an externally imposed oscillatory shear flow is explored by theory and computer simulation. The special case of a single trapped particle is solved analytically. We present explicit results for the time-dependent density and the velocity distribution. The response of the many-body problem is studied by computer simulations. In particular, we investigate the influence of oscillatory shear flow on the internal modes of the cluster. As a function of the shear oscillation frequency, we find resonant behavior for certain (antisymmetric) normal modes, implying that they can be efficiently excited by oscillatory shear. Our results are verifiable in experiments on dusty plasmas and trapped colloidal dispersions.

I. INTRODUCTION

Recently, it has become possible to trap mesoscopic classical dust grains or colloidal spheres in external fields (e.g., laser-optical tweezers, electric fields, or thermal fields [1]), where they form well-controlled clusters containing only a few particles [2–5]. In many cases, the effective confinement potential is practically harmonic. For a dusty plasma, it has been shown that the cluster typically possesses a shell structure [6–11] and exhibits a melting transition upon heating [12]. Dynamically, there are internal modes like breathing [13] and rotation excitations [14], which can be induced either thermally, by lasers [15], or by adding a second delocalizing time-dependent field [16]. A similar setup can be realized for colloidal dispersions in a fluid solvent, where the same phenomena are observed, albeit with the caveat that the damping of the particles is much larger. Hard-sphere-like colloids have been confined to cavities, and the glass transition has been studied [17–20]. The clusters can be two-dimensional both for dusty plasmas and colloids. In the latter case, superparamagnetic particles have been used in a circular environment [21].

Here, we put forward the idea of exposing a cluster of trapped Brownian particles to an external oscillatory shear flow field. Shear flow can be imposed on both dusty plasma and colloidal clusters: For dusty plasmas, a rotating electrode can be used to induced a flow field of the neutral gas, which then exerts an additional friction term relative to the flow field [22–24]. In the colloidal case, the solvent can be directly sheared in shear cells [25,26].

The simplest case is steady-state linear shear (Couette flow), where the flow field is time independent. Oscillatory shear fields with a characteristic oscillation frequency Ω can also be imposed: For dusty plasmas, this would be an oscillatory electrode, a setup that has not yet been implemented but which is, in principle, conceivable. In the colloidal context, oscillatory shear is a standard rheological setup which also has been used in particle-resolved studies [27–29]. Our goal here is to predict, by theory and simulation, the response of a finite trapped particle cluster to oscillatory shear.

Our motivation to do so is threefold: First, the oscillation frequency Ω inherent in the shear excitation can excite certain dynamic modes. A selective excitation of modes would be helpful to understand and control the dynamic response of the whole cluster. This could be pivotal to constructing new antenna systems, for example, ultrasonic emitters [30]. Second, more fundamentally, even the case of a single trapped particle is interesting since analytical solutions have been presented for the linear-shear case [31–34]. Due to the stochastic Brownian force, these solutions are nontrivial and exhibit interesting particle distribution functions and shear-induced cross-correlations. Here, we generalize the analytical solution to oscillatory shear and discuss the dependence on the shear oscillation frequency Ω. The analytical solution is already interesting in itself since it may serve as a standard situation to compare with the many-body system. Third, our predictions are verifiable in experiments on complex plasmas or on colloids. This concerns the behavior of a single particle (as predicted by our analytical solution) and that of many particles (as predicted by our simulations).

A colloid experiment is in principle straightforward and has already been implemented to verify the analytically predicted behavior of two particles in time-independent shear flow [35]. This has been done with the caveat that the hydrodynamic interactions between the particles play an important role for more than a single particle in the trap [16,36,37]. The latter are irrelevant for gas flow in complex plasmas, where oscillatory shear can be imposed by a time-oscillating electrode [22,23].

As a result, our analytical solutions reveal that the particle and velocity distributions exhibit a strong resonance in weakly damped systems. With relatively low shear rates, it is possible to induce a significant anisotropy in the distribution functions. Our simulations for a small cluster show that oscillatory shear can be used to excite particular modes in confined systems. This is demonstrated for four particles, where we observe two resonances for the amplitude of the spatial cross-moment.

This paper is organized as follows: The theoretical model and the relevant equations are introduced in Sec. II. The solution for the single-particle problem is worked out in Sec. III. In particular, we derive explicit solutions for the time-dependent moments of the position and velocity distribution functions. In Sec. IV, Langevin dynamics simulations are
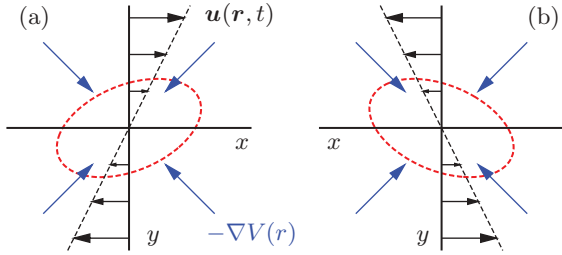
---

*hlowen@thphy.uni-duesseldorf.de

FIG. 1. (Color online) Sketch of the flow field $\boldsymbol{u}(\boldsymbol{r},t)$, the confining force $-\nabla V(r)$, and the particle distribution (ellipse) at (a) $t = t_0$ and (b) $t = t_0 + T_{\text{sh}}/2$.

performed to study the effect of oscillatory shear on strongly interacting few-particle systems. We conclude with a summary and discussion of our results in Sec. V. Mathematical details and the explicit results for the moments are presented in the Appendices.

II. MODEL

We consider N particles with identical mass m that are confined by an isotropic harmonic confinement potential

$$V(r) = \frac{m}{2}\omega_0^2 r^2, \tag{1}$$

where ω_0 is the trap frequency and $r^2 = x^2 + y^2$. They are subject to an oscillatory shear flow described by the velocity field

$$\boldsymbol{u}(\boldsymbol{r},t) = \dot{\gamma} y \cos(\Omega t)\, \hat{\mathbf{e}}_x, \tag{2}$$

with $\hat{\mathbf{e}}_x$ denoting the unit vector in the x direction, $\dot{\gamma}$ the shear rate, and Ω the shear frequency (period $T_{\text{sh}} = 2\pi/\Omega$). The model is illustrated in Fig. 1.

The dynamics of N particles is described by the Langevin equations

$$\ddot{\boldsymbol{r}}_i = -\omega_0^2 \boldsymbol{r}_i + \sum_{j \neq i}^{N} \frac{\boldsymbol{F}(\boldsymbol{r}_{ij})}{m} - \nu[\dot{\boldsymbol{r}}_i - \boldsymbol{u}(\boldsymbol{r}_i,t)] + \frac{\boldsymbol{f}_i}{m}, \tag{3}$$

where $\boldsymbol{F}(\boldsymbol{r}_{ij})$ is the interparticle force, ν is the damping coefficient, and $\boldsymbol{f}_i(t) = (f_i^x(t), f_i^y(t))^T$ the stochastic force. The latter is assumed to have zero mean, $\langle \boldsymbol{f}_i(t) \rangle = 0$, and the correlation function

$$\left\langle f_i^{\alpha}(t) f_j^{\beta}(t') \right\rangle = 2m\nu k_{\text{B}} T_{\text{n}} \delta_{ij}\delta^{\alpha\beta}\, \delta(t - t'). \tag{4}$$

Here, T_{n} denotes the neutral gas temperature and k_{B} denotes the Boltzmann constant. Particle indices are labeled by $i, j \in \{1, \ldots, N\}$ and coordinates by $\alpha, \beta \in \{x, y\}$.

In the static limit ($\Omega = 0$), several aspects of this problem have been addressed previously, for example, diffusion [38], inertial effects [31], dynamic properties [33], fluctuation-dissipation relations [34,39], the probability distribution in the overdamped limit [32], or retardation effects [40]. In the following, we focus on the oscillatory case with $\Omega > 0$ and explore the influence of the periodic flow on the dynamics of a single particle (Sec. III) and many particles (Sec. IV).

III. SINGLE-PARTICLE PROBLEM

In this section, the motion of a single particle is investigated analytically by solving the Langevin equation (3).

A. Solution of Langevin equation

The two second-order equations (3) can be written equivalently as the following system of first-order equations for $\boldsymbol{\chi}(t) = (v_x(t), v_y(t), x(t), y(t))^T$,

$$\dot{\boldsymbol{\chi}}(t) = \boldsymbol{A}(t)\boldsymbol{\chi}(t) + \boldsymbol{\xi}(t). \tag{5}$$

Here, we have introduced $\boldsymbol{\xi}(t) = (f_x(t), f_y(t), 0, 0)^T/m$ with

$$\langle \boldsymbol{\xi}(t) \rangle = 0, \qquad \langle \boldsymbol{\xi}(t)\boldsymbol{\xi}^T(t') \rangle = \boldsymbol{D}\,\delta(t - t'), \tag{6}$$

where the diffusion matrix is given by

$$\boldsymbol{D} = \frac{2\nu k_{\text{B}} T_{\text{n}}}{m} \begin{pmatrix} 1 & 0 & 0 & 0 \\ 0 & 1 & 0 & 0 \\ 0 & 0 & 0 & 0 \\ 0 & 0 & 0 & 0 \end{pmatrix}. \tag{7}$$

Compared to static shear flow [31,34], the coefficient matrix $\boldsymbol{A}(t)$ now becomes time dependent and reads

$$\boldsymbol{A}(t) = \begin{pmatrix} -\nu & 0 & -\omega_0^2 & \nu\dot{\gamma}\cos(\Omega t) \\ 0 & -\nu & 0 & -\omega_0^2 \\ 1 & 0 & 0 & 0 \\ 0 & 1 & 0 & 0 \end{pmatrix}. \tag{8}$$

Note that it is T_{sh} periodic; that is, $\boldsymbol{A}(t + T_{\text{sh}}) = \boldsymbol{A}(t)$. In mathematical terms, Eq. (5) describes an Ornstein-Uhlenbeck process with time-periodic coefficients; see Refs. [41,42] for more general investigations.

The solution of a system of linear ordinary differential equations such as Eq. (5) with the initial condition $\boldsymbol{\chi}(t_0) = \boldsymbol{\chi}_0$ can be written in the form (see, e.g., Ref. [43])

$$\begin{aligned} \boldsymbol{\chi}(t) &= \boldsymbol{U}(t)\boldsymbol{\chi}_0 + \boldsymbol{U}(t)\int_{t_0}^{t} \boldsymbol{U}^{-1}(t')\boldsymbol{\xi}(t')\, dt' \\ &= \boldsymbol{G}(t,t_0)\boldsymbol{\chi}_0 + \int_{t_0}^{t} \boldsymbol{G}(t,t')\boldsymbol{\xi}(t')\, dt', \end{aligned} \tag{9}$$

where $\boldsymbol{U}(t)$ represents the solution of the homogeneous equation ($\boldsymbol{\xi} \equiv 0$). It satisfies $\dot{\boldsymbol{U}}(t) = \boldsymbol{A}(t)\boldsymbol{U}(t)$ and $\boldsymbol{U}(t_0) = \mathbf{1}$ with $\mathbf{1}$ being the unit matrix. The second line is an equivalent expression (see, e.g., Refs. [41,42]) in terms of the evolution operator

$$\boldsymbol{G}(t,t') = \boldsymbol{U}(t)\boldsymbol{U}^{-1}(t'). \tag{10}$$

The explicit results for $\boldsymbol{U}(t)$ are derived in Appendix A.

B. Mean and correlation functions

From Eqs. (6) and (9) we can calculate the mean value (see Ref. [31])

$$\langle \boldsymbol{\chi}(t) \rangle = \boldsymbol{U}(t)\boldsymbol{\chi}_0 \tag{11}$$

and the correlation matrix ($\tau > 0$)

$$C(t,\tau) = \langle [\chi(t+\tau) - \langle \chi(t+\tau) \rangle][\chi(t) - \langle \chi(t) \rangle]^T \rangle$$
$$= \int_{t_0}^{t} dt' \, G(t+\tau,t') D \, G^T(t,t'). \qquad (12)$$

Our interest is in the stationary state ("s") at times $t - t_0 \gg \nu^{-1}$ when the system has lost any memory of the initial conditions. For this purpose we let $t_0 \to -\infty$,

$$C_s(t,\tau) = \int_{-\infty}^{t} dt' \, G(t+\tau,t') D \, G^T(t,t')$$
$$= U(t+\tau) \left[\int_{-\infty}^{t} dt' \, U^{-1}(t') D \, (U^{-1})^T(t') \right] U^T(t). \qquad (13)$$

Due to the periodicity of $A(t)$, the evolution operator is invariant under a time shift by T_{sh} [41]; that is, $G(t + T_{sh}, t' + T_{sh}) = G(t,t')$. By changing the integration variable in Eq. (13) and making use of the periodicity, one can then show that $C_s(t + T_{sh}, \tau) = C_s(t,\tau)$. As a consequence of the symmetry of the shear flow, the mean value [Eq. (11)] vanishes: $\langle \chi(t) \rangle_s = 0$.

Since the motion in the y direction is independent of the shear flow, the respective correlation functions remain unaffected. They are simply those of a damped harmonic oscillator and can be found, for example, in Ref. [44]. All other cases are evaluated from Eq. (13) and the explicit results for $U(t)$ given in Appendix A (with the help of computer algebra).[1]

C. Moments of the distribution function

In the following, we consider the static ($\tau = 0$) correlation functions of $\chi(t)$, that is, the second moments that determine the (Gaussian) distribution function; see Refs. [31,33]. They can be written as [cf. Eq. (13)]

$$C_s(t,0) = \frac{k_B T_n}{m\omega_0^2} \left[\text{diag}(\omega_0^2, \omega_0^2, 1, 1) \right.$$
$$\left. + \text{Wi}^2 \, \text{diag}(\omega_0^2 d_{v_x}, 0, d_x, 0) + \text{Wi} \, R(t) \right], \qquad (14)$$

where $\text{Wi} = \dot{\gamma}\nu/\omega_0^2$ is the Weissenberg number [33]. The time-independent contributions are given by

$$d_x = \frac{\bar{\Omega}^2 + 4(\bar{\nu}^2 + 1)}{(\bar{\nu}^2 + \bar{\Omega}^2)[4\bar{\nu}^2\bar{\Omega}^2 + (\bar{\Omega}^2 - 4)^2]}, \qquad (15)$$

$$d_{v_x} = \frac{1}{2} \frac{\bar{\Omega}^4 + 2(2\bar{\nu}^2 - 1)\bar{\Omega}^2 + 8}{(\bar{\nu}^2 + \bar{\Omega}^2)[4\bar{\nu}^2\bar{\Omega}^2 + (\bar{\Omega}^2 - 4)^2]}, \qquad (16)$$

where $\bar{\Omega} = \Omega/\omega_0$ and $\bar{\nu} = \nu/\omega_0$. For future reference we introduce the dimensionless shear rate $\dot{\bar{\gamma}} = \dot{\gamma}/\omega_0$. The explicit results for the time-dependent contributions $R(t) = R(t + T_{sh})$ are presented in Appendix B. Note that the matrix is symmetric, $C_s(t,0) = C_s^T(t,0)$.

―――――――

[1] If we choose the limit $t_0 \to -\infty$ such that $t_0 = t_0^* = -nT_{sh}$ with $n \in \mathbb{N}$, $n \to \infty$, we have $G(t,t') = G(t + t_0^*, t' + t_0^*) = U(t + t_0^*) U^{-1}(t' + t_0^*)$. The matrix $U(t)$ explicitly depends on t and t_0; i.e., $U(t) = U_{t_0}(t)$. From Eqs. (A8) and (A9) one can see that $U_{t_0^*}(t + t_0^*) = U_0(t)$, which we use to evaluate the integral in Eq. (13).

1. Angular momentum and rotation

In the static limit, it is known that the flow leads to rotation with a constant angular momentum [31]. In the time-dependent case, it is given by

$$\langle L_z(t) \rangle = m \langle xv_y - yv_x \rangle$$
$$= -\frac{k_B T_n}{\omega_0} \frac{\dot{\bar{\gamma}}}{\sqrt{1 + (\Omega/\nu)^2}} \cos(\Omega t + \phi_{L_z}), \quad (17)$$

where $\varphi_{L_z} = -\arctan(\Omega/\nu)$ is the phase angle. Note that the amplitude is negative.

The angular momentum is largely determined by the ratio of the shear frequency and the damping rate. If the latter significantly exceeds the former ($\Omega/\nu \ll 1$), the phase shift φ_{L_z} vanishes, and the amplitude is slightly smaller than in the static limit ($\Omega = 0$) [31]. On the other hand, if $\Omega/\nu \gg 1$, the phase shift asymptotically tends to $-\pi/2$ while the amplitude decreases monotonically and goes to zero.

2. Resonances

The shear flow can be considered an external periodic driving force. As such, it allows excitation of internal modes of the unperturbed system both in the linear and nonlinear regime. We now explicitly consider the spatial and velocity moments, where resonance effects manifest themselves as amplitude peaks at particular excitation (i.e., shear) frequencies.

Since the y component is not directly affected by the shear flow, its moments are $\langle y^2 \rangle = k_B T_n/(m\omega_0^2)$ and $\langle v_y^2 \rangle = k_B T_n/m$. Using the results presented in Appendix B, one finds for the cross moments

$$\langle x(t)y(t) \rangle = \text{Wi}\left(\frac{k_B T_n}{m\omega_0^2}\right) A_{xy} \cos(\Omega t + \phi_{xy}), \qquad (18)$$

$$\langle v_x(t)v_y(t) \rangle = \text{Wi}\left(\frac{k_B T_n}{m}\right) A_{v_x v_y} \cos(\Omega t + \phi_{v_x v_y}), \quad (19)$$

where the amplitudes are given by

$$A_{xy} = \left[\frac{4\bar{\nu}^2 + \bar{\Omega}^2}{(\bar{\nu}^2 + \bar{\Omega}^2)[4\bar{\nu}^2\bar{\Omega}^2 + (\bar{\Omega}^2 - 4)^2]}\right]^{1/2}, \qquad (20)$$

$$A_{v_x v_y} = \left[\frac{\bar{\Omega}^2}{(\bar{\nu}^2 + \bar{\Omega}^2)[4\bar{\nu}^2\bar{\Omega}^2 + (\bar{\Omega}^2 - 4)^2]}\right]^{1/2}, \qquad (21)$$

and the phase angles follow from

$$\tan\phi_{xy} = \bar{\nu}\bar{\Omega}\left[\frac{\bar{\Omega}^2 + 4(\bar{\nu}^2 + 1)}{\bar{\Omega}^4 - 4\bar{\Omega}^2 + 4\bar{\nu}^2(\bar{\Omega}^2 - 2)}\right], \qquad (22)$$

$$\tan\phi_{v_x v_y} = \frac{\bar{\nu}}{\bar{\Omega}}\left[\frac{3\bar{\Omega}^2 - 4}{\bar{\Omega}^2 - 2\bar{\nu}^2 - 4}\right]. \qquad (23)$$

Similarly, we get

$$\frac{\langle x^2(t) \rangle}{k_B T_n/m\omega_0^2} = 1 + \text{Wi}^2[d_x + A_{xx}\cos(2\Omega t + \phi_{xx})], \qquad (24)$$

$$\frac{\langle v_x^2(t) \rangle}{k_B T_n/m} = 1 + \text{Wi}^2[d_{v_x} + A_{v_x v_x}\cos(2\Omega t + \phi_{v_x v_x})], \qquad (25)$$

with rather complicated expressions for the amplitudes and phase angles:

$$A_{xx} = \left[\frac{4\bar{v}^4 + 4(\bar{\Omega}^2 - 1)^2 + \bar{v}^2(17\bar{\Omega}^2 + 8)}{4(\bar{v}^2 + \bar{\Omega}^2)(\bar{v}^2 + 4\bar{\Omega}^2)[4v^2\bar{\Omega}^2 + (\bar{\Omega}^2 - 4)^2][\bar{v}^2\bar{\Omega}^2 + (\bar{\Omega}^2 - 1)^2]} \right]^{1/2}, \tag{26}$$

$$A_{v_x v_x} = \left[\frac{4\bar{v}^4\bar{\Omega}^4 + 4(\bar{\Omega}^2 - 1)^4 + \bar{v}^2\bar{\Omega}^2(17\bar{\Omega}^4 - 4\bar{\Omega}^2 - 4)}{4(\bar{v}^2 + \bar{\Omega}^2)(\bar{v}^2 + 4\bar{\Omega}^2)[4\bar{v}^2\bar{\Omega}^2 + (\bar{\Omega}^2 - 4)^2][\bar{v}^2\bar{\Omega}^2 + (\bar{\Omega}^2 - 1)^2]} \right]^{1/2}, \tag{27}$$

$$\tan\phi_{xx} = \bar{v}\bar{\Omega}\left(\frac{8\bar{\Omega}^6 - 22\bar{\Omega}^4 + 38\bar{\Omega}^2 - 24 + 4\bar{v}^4(2\bar{\Omega}^2 - 3) + \bar{v}^2(34\bar{\Omega}^4 - 31\bar{\Omega}^2 - 16)}{4\bar{\Omega}^2(\bar{\Omega}^2 - 4)(\bar{\Omega}^2 - 1)^2 - 4\bar{v}^6\bar{\Omega}^2 - \bar{v}^4(13\bar{\Omega}^4 + 20\bar{\Omega}^2 - 8) - \bar{v}^2(-13\bar{\Omega}^6 + 41\bar{\Omega}^4 + 10\bar{\Omega}^2 - 8)} \right), \tag{28}$$

$$\tan\phi_{v_x v_x} = \bar{v}\bar{\Omega}\left(\frac{8\bar{\Omega}^8 - 36\bar{\Omega}^6 + 90\bar{\Omega}^4 - 86\bar{\Omega}^2 + 24 + 8\bar{v}^4\bar{\Omega}^2(\bar{\Omega}^2 - 1) + \bar{v}^2(34\bar{\Omega}^6 - 41\bar{\Omega}^4 + 4)}{4\bar{\Omega}^2(\bar{\Omega}^2 - 4)(\bar{\Omega}^2 - 1)^3 - 4\bar{v}^6\bar{\Omega}^4 - \bar{v}^4\bar{\Omega}^4(13\bar{\Omega}^2 + 6) - \bar{v}^2(-13\bar{\Omega}^8 + 31\bar{\Omega}^6 + 30\bar{\Omega}^4 - 38\bar{\Omega}^2 + 8)} \right). \tag{29}$$

The results for the cross-moments are illustrated in Fig. 2. For weak damping, both A_{xy} and $A_{v_x v_x}$ exhibit a clear resonance near $\bar{\Omega} = 2$, which becomes less pronounced as the damping rate increases. While $A_{v_x v_y} \to 0$ for $\bar{\Omega} \to 0$, A_{xy} approaches a constant value in the static limit. The dependence of the phase angles on the shear frequency is monotonic, except for ϕ_{xy}, which displays a small minimum at weak damping and low $\bar{\Omega}$; see Fig. 2(a). In the high-frequency limit, both amplitudes go to zero.

Compared to the cross-moments, the amplitudes for the time-dependent contributions to $\langle x^2(t) \rangle$ and $\langle v_x^2(t) \rangle$ have a two-peak structure at low damping; see Fig. 3. In addition to the maximum near $\bar{\Omega} = 2$, they exhibit another peak near the trap frequency, $\bar{\Omega} = 1$, which can become the dominant resonance at intermediate damping; see Fig. 3(a). The constant terms d_x and d_{v_x}, on the other hand, have only a single peak near $\bar{\Omega} = 2$. Both the constant terms and the amplitudes attain large values near the static limit and the resonance frequency. They vanish in the limit $\bar{\Omega} \to \infty$.

3. Particle and velocity distribution

We now turn to the details of the spatial and velocity distribution functions. A principal component analysis [33] yields the lengths of the principal axes $\sqrt{c_{p,v;1,2}}$ of the elliptical distributions and their orientation in space, characterized by the angle $\phi_{p,v}(t)$ between the longer axis and the x axis. The ratio $V_{p,v}(t)$ between the two axes and the angle $\phi_{p,v}(t)$ are determined by [33]

$$c_{p;1,2}(t) = \frac{1}{2}[\langle x^2 \rangle + \langle y^2 \rangle \pm \sqrt{4\langle xy \rangle^2 + (\langle x^2 \rangle - \langle y^2 \rangle)^2}],$$

$$\tan\phi_p(t) = \frac{1}{2}\left[\frac{\langle xy \rangle}{|\langle xy \rangle|} \sqrt{4 + \left(\frac{\langle x^2 \rangle - \langle y^2 \rangle}{\langle xy \rangle} \right)^2} - \left(\frac{\langle x^2 \rangle - \langle y^2 \rangle}{\langle xy \rangle} \right) \right], \tag{30}$$

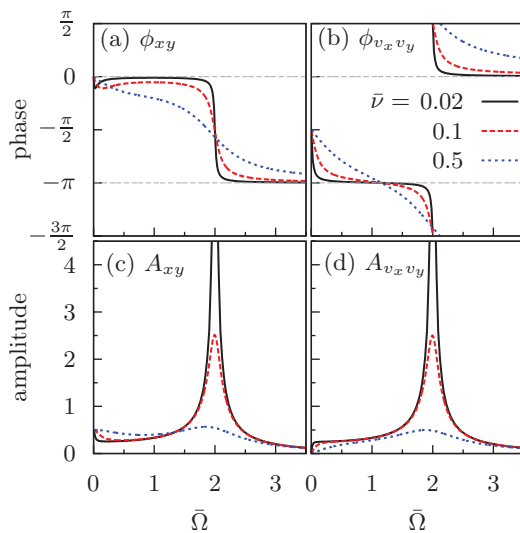$$V_p(t) = \sqrt{\frac{c_{p;2}}{c_{p;1}}}, \tag{31}$$

FIG. 2. (Color online) Phase angles [(a), (b)] and amplitudes [(c), (d)] of $\langle x(t)y(t) \rangle$ and $\langle v_x(t)v_y(t) \rangle$ according to Eqs. (20)–(23) for the parameters indicated in the figure.
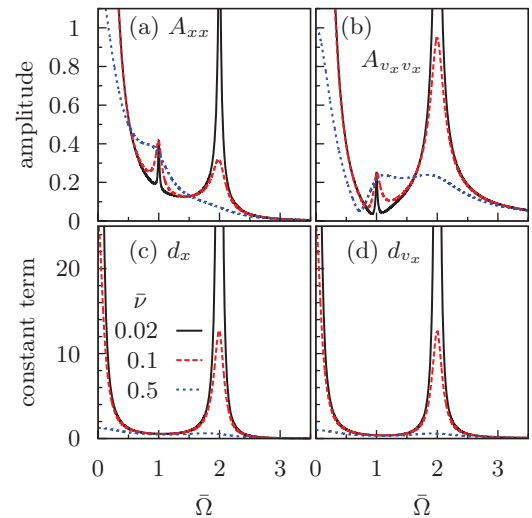

FIG. 3. (Color online) Amplitudes [(a), (b)] and constant terms [(c), (d)] of $\langle x^2(t) \rangle$ and $\langle v_x^2(t) \rangle$ according to Eqs. (26) and (27) and Eqs. (15) and (16) for the parameters indicated in the figure.

where the subscript 1 (2) refers to the plus (minus) sign. The expressions for the velocity distribution are analogous.

Before we study the time evolution, we compare our results for the static limit $\Omega = 0$,

$$\tan \phi_p = \sqrt{1 + \frac{1}{4}\left(\text{Wi} + \frac{\dot{\gamma}}{\nu}\right)^2} - \frac{1}{2}\left(\text{Wi} + \frac{\dot{\gamma}}{\nu}\right), \quad (32)$$

$$V_p = \left[\frac{\text{Wi} + \frac{\dot{\gamma}}{\nu} + \frac{4}{\text{Wi}} - \sqrt{4 + \left(\text{Wi} + \frac{\dot{\gamma}}{\nu}\right)^2}}{\text{Wi} + \frac{\dot{\gamma}}{\nu} + \frac{4}{\text{Wi}} + \sqrt{4 + \left(\text{Wi} + \frac{\dot{\gamma}}{\nu}\right)^2}}\right]^{1/2}, \quad (33)$$

with previous calculations [31,33,34]. Holzer *et al.* [33] considered the overdamped limit. Consequently, their results do not account for the $\sim \dot{\gamma}/\nu$ correction terms that are important in weakly damped systems. Rzehak and Zimmermann [31], on the other hand, explicitly considered inertial effects but used an adjusted diffusion matrix that incorporated properties of the flow field. Their results then agree with ours for $\dot{\gamma}/\nu = 0$ and those of Ref. [33] for the overdamped case. For the velocity distribution one finds $\phi_v = 0$ and an increased kinetic temperature in the flow direction,

$$V_v = \left[1 + \frac{\dot{\gamma}^2}{2}\right]^{-1/2}; \quad (34)$$

see Refs. [31,34]. It is independent of the damping rate ν.

Since the time-dependent contributions to the second moments vanish in the high-frequency limit, $\bar{\Omega} \to \infty$, we obtain $V_{p,v} \to 1$. Here, the particles are too inert to adjust to the motion of the flow.

At finite shear frequencies, the angle $\phi_{p,v}(t)$ satisfies $\phi_{p,v}(t + T_{\text{sh}}/2) = -\phi_{p,v}(t)$, while the ratio of the axes is strictly $T_{\text{sh}}/2$ periodic, $V_{p,v}(t + T_{\text{sh}}/2) = V_{p,v}(t)$. The time evolution is depicted in Figs. 4–7. Generally, the maximum

FIG. 5. (Color online) Ratio between the minor and the major axis of the particle distribution according to Eq. (31) for $\dot{\gamma} = 0.2$ (solid line), $\dot{\gamma} = 1$ (long-dashed line), and $\dot{\gamma} = 5$ (short-dashed line).

value the angle can attain decreases with the shear rate, which is accompanied by an increasingly elongated particle and velocity distribution.

We first discuss the results for the particle (density) distribution. Near the static limit, $\phi_p(t)$ shows the most complicated behavior. For sufficiently high shear or damping rates, the angle can feature two minima and maxima during
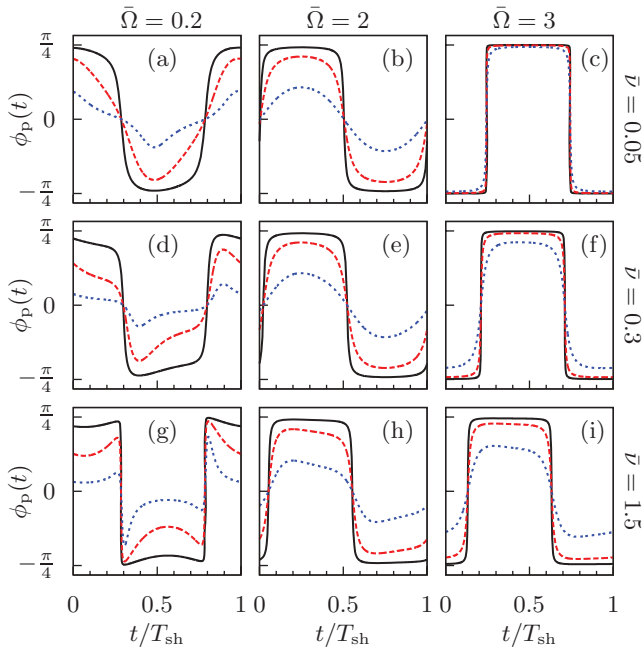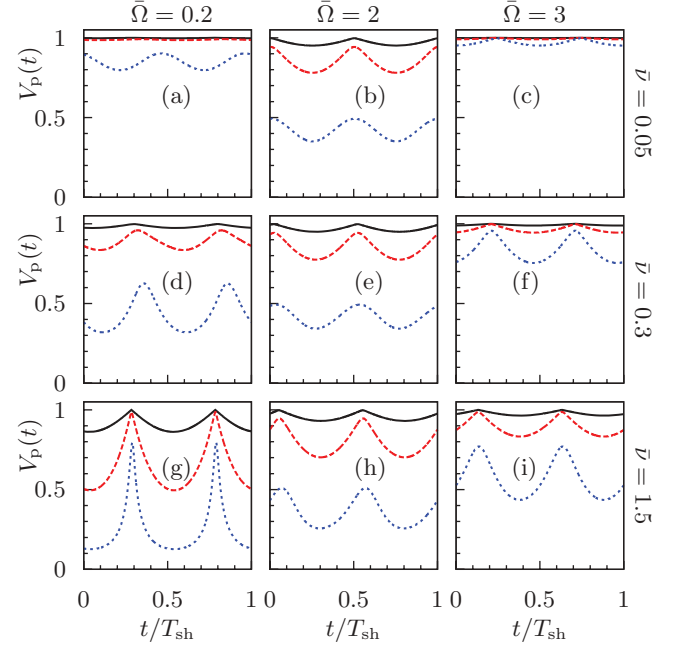

FIG. 4. (Color online) Angle between the major axis and the x axis of the particle distribution according to Eq. (30) for $\dot{\gamma} = 0.2$ (solid line), $\dot{\gamma} = 1$ (long-dashed line), and $\dot{\gamma} = 5$ (short-dashed line).
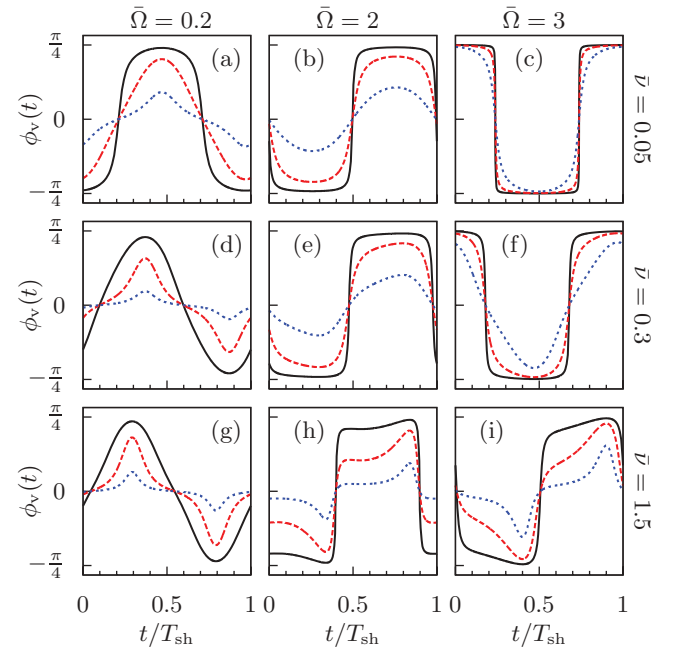

FIG. 6. (Color online) Angle between the major axis and the x axis of the velocity distribution for $\dot{\gamma} = 0.2$ (solid line), $\dot{\gamma} = 1$ (long-dashed line), and $\dot{\gamma} = 5$ (short-dashed line).
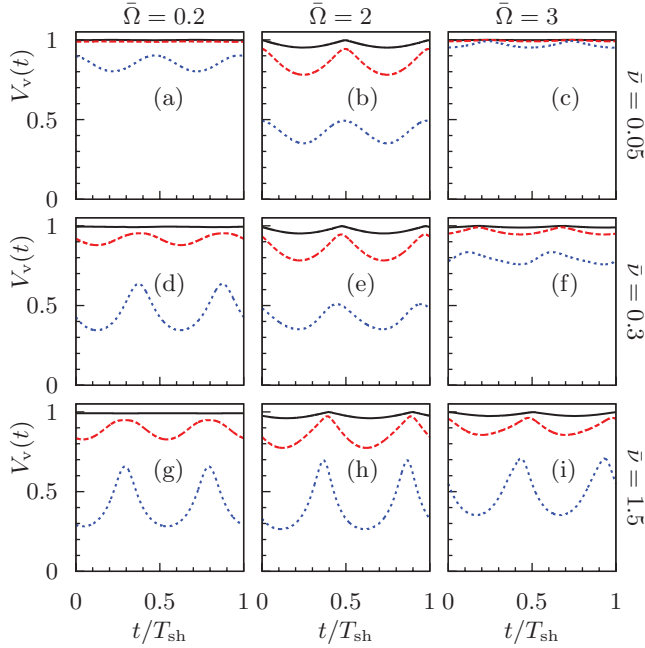
FIG. 7. (Color online) Ratio between the minor and the major axis of the velocity distribution for $\dot{\gamma} = 0.2$ (solid line), $\dot{\gamma} = 1$ (long-dashed line), and $\dot{\gamma} = 5$ (short-dashed line).

FIG. 8. (Color online) Dependence of $\hat{A}_{xy}$ on the shear frequency for $\bar{v} = 0.1$. The squares ($\dot{\gamma} = 0.3$) and circles ($\dot{\gamma} = 0.8$) show results for $N = 4$ particles with $\Gamma = 400$ and $a/\lambda = 0.7$. In these cases, the length scale on the vertical axis must read $l_0 = a$. The vertical lines show the eigenfrequencies of the modes sketched in the right part of the figure [24,46]. The triangles denote simulation results for noninteracting particles ($N = 500$, $\dot{\gamma} = 1$), where the associated length scale reads $l_0^2 = k_B T_n/(m\omega_0^2)$. The solid line (blue [gray]) shows the corresponding analytical result; see Eqs. (18) and (20).

a shear cycle; see Fig. 4(g). In these cases, $V_p(t)$ exhibits the largest variations and closely approaches zero at high $\dot{\gamma}$ [Fig. 5(g)]. The shape of the distribution changes from almost spherical to very elongated. Since Ω/ν is small, the amplitude of the mean angular momentum is large and close to the value in the static limit; see Eq. (17). In the high frequency limit ($\bar{\Omega} = 3$), the angle quickly changes its sign and has an almost stepwise behavior, which becomes less pronounced at higher shear or damping rates. A high shear rate leads to a more permanent elongation of the distribution than near the static limit.

Resonance effects can be observed in Figs. 5(a)–5(c), where the damping rate is low ($\bar{v} = 0.05$). Close to the resonance frequency ($\bar{\Omega} = 2$), an increase of the shear rate leads to a significant reduction of V_p [Fig. 5(b)], while the decrease in the high- and low-frequency limits is considerably weaker [Figs. 5(a) and 5(c)]. The effect becomes much less obvious at higher damping rates, where the resonance is suppressed, and the distribution in the low-frequency limit becomes more elongated for identical flow parameters.

Let us now consider the corresponding parameters for the velocity distribution, which are depicted in Figs. 6 and 7. At low frequencies and high shear rates, the angle $\phi_v(t)$ shows a pronounced extremum during a half-cycle. Near the resonance frequency and rather high damping, we observe a two-peak structure similar to that of ϕ_p at low frequencies. The behavior at $\bar{\Omega} = 3$ is still similar, but the two-peak structure vanishes. The behavior of $V_v(t)$ is very similar to that of $V_p(t)$. One recognizes the resonance at $\bar{\Omega} = 2$ and $\bar{v} = 0.05$, where V_v is much more affected by a variation of the shear rate than at $\bar{\Omega} = 0.2$ and $\bar{\Omega} = 3$. In the low-frequency case, the elongation of the velocity distribution is less pronounced than the elongation of the particle distribution.
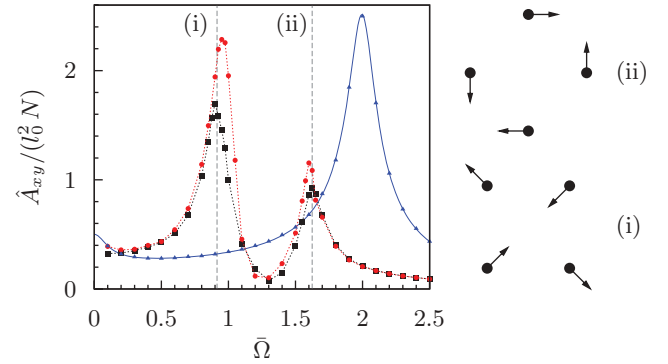
IV. MANY-BODY EFFECTS

In this section, we approach the many-body problem by Langevin dynamics simulations.[2] As an example, we investigate a cluster with four particles, which has been the subject of previous studies in the context of dusty plasmas [14,46]. For the particle interactions, which give rise to new collective phenomena compared to the single-particle problem studied in the previous section, we employ the Yukawa potential $\phi(r) = Q^2 \exp(-r/\lambda)/r$, where λ denotes the screening length and Q denotes the particle charge. This pairwise interaction neglects the physical core size of the particles.

Our simulations are done for the underdamped case found in dusty plasmas. Note that for the overdamped colloid dynamics, hydrodynamic interactions [5,26] between colloidal particles become relevant, including lubrication forces at contact, which are not considered in this paper.

At strong coupling conditions—characterized by $\Gamma = Q^2/(ak_B T_n) \gg 1$, where $a = (Q^2/m\omega_0^2)^{1/3}$—the linear response of the cluster is described by its $2N$ normal modes. They are obtained from a diagonalization of the Hessian matrix [47]. In the following, we show that oscillatory shear flow can be used to excite particular modes of the system.

The normal modes of the four-particle cluster have been studied previously [14,24,46]. They contain two antisymmetric excitations that compress the cluster in one direction and elongate it in the other; see Fig. 8. There, we show

$$\hat{A}_{xy} = \left(\frac{2/\text{Wi}^2}{T_{sh}} \int_0^{T_{sh}} [\langle x(t)y(t) \rangle - \langle x(t) \rangle \langle y(t) \rangle]^2 dt \right)^{1/2} \quad (35)$$

as obtained from an average over many shear periods.

For the low shear rate ($\dot{\gamma} = 0.3$), the location of the peaks is in very good agreement with the frequencies of the aforementioned eigenmodes, which shows that they are responsible

---

[2]We use the "symplectic low-order algorithm" (SLO) of Ref. [45].

for the resonance. As the shear rate increases ($\dot{\bar{\gamma}} = 0.8$), we observe a small shift of the resonance frequencies, which could be caused by nonlinear effects. Here, the excitation becomes stronger, and the shear flow considerably disturbs the cluster. The high-frequency behavior of the amplitude is only marginally affected by the shear rate, and the two curves for $\dot{\bar{\gamma}} = 0.3$ and $\dot{\bar{\gamma}} = 0.8$ merge. Temperature is expected to smear out the resonances but not to drive nonlinear stochastic resonances [48]. Clearly, we recover the amplitude predicted by Eq. (20) for noninteracting particles.

V. CONCLUSION

In summary, we have derived the analytical solution for harmonically trapped particles in oscillatory linear shear flow. While we have focused on the moments of the distribution function, our results can also be used to explicitly calculate the correlation functions. We have shown that the flow field leads to a time-dependent variation of the aspect ratio of the principal axes and their orientation in space. As a function of the shear frequency, the cross-moments show resonant behavior near $\bar{\Omega} = 2$.

Our simulations have shown that resonances also occur in many-particle systems. In particular, oscillatory shear flow allows excitations of particular normal modes, where the cluster is being compressed in one direction and elongated in the other. This has been demonstrated for a small cluster but should be equally efficient in larger systems with hundreds of particles. The effect could be used to excite and probe the linear and nonlinear response of confined dusty plasmas and their dependence on temperature, screening, etc.

Finally, the model can also be generalized to active Brownian particles; see Ref. [49] for a recent review. In this case, a negative friction is used to keep the particle on a nonvanishing velocity [50].

APPENDIX A: SOLUTION OF HOMOGENEOUS EQUATION

The solution matrix $\boldsymbol{U}(t)$ for Eq. (5) can be found by first considering the motion in the y direction only, which is completely decoupled from the motion in the flow direction. Since we only require the solution for $\boldsymbol{\xi} \equiv 0$ (the homogeneous equation), the stochastic force can be omitted in the following. The y component now satisfies the equation of motion of a damped harmonic oscillator. In the x direction, however, the flow field acts as an additional driving force:

$$\ddot{y}_{\mathrm{h}}(t) + \nu \dot{y}_{\mathrm{h}}(t) + \omega_0^2 y_{\mathrm{h}}(t) = 0 \tag{A1}$$

$$\ddot{x}_{\mathrm{h}}(t) + \nu \dot{x}_{\mathrm{h}}(t) + \omega_0^2 x_{\mathrm{h}}(t) = \nu \dot{\gamma} \cos(\Omega t) y_{\mathrm{h}}(t). \tag{A2}$$

The solution $\boldsymbol{y}_{\mathrm{h}}(t) = (v_{y,\mathrm{h}}(t), y_{\mathrm{h}}(t))^T$ with the initial condition $\boldsymbol{y}_{\mathrm{h}}(t_0) = \boldsymbol{y}_0$ can then be written in the form

$$\boldsymbol{y}_{\mathrm{h}}(t) = \boldsymbol{H}(t - t_0) \boldsymbol{y}_0, \tag{A3}$$

where $\boldsymbol{H}(t)$ contains the well-known solution for the under-damped harmonic oscillator,

$$\boldsymbol{H}(t) = e^{-\beta t}$$
$$\times \begin{pmatrix} \cos(\omega_{\mathrm{r}} t) - \frac{\beta}{\omega_{\mathrm{r}}} \sin(\omega_{\mathrm{r}} t) & -\omega_0^2 \sin(\omega_{\mathrm{r}} t)/\omega_{\mathrm{r}} \\ \sin(\omega_{\mathrm{r}} t)/\omega_{\mathrm{r}} & \cos(\omega_{\mathrm{r}} t) + \frac{\beta}{\omega_{\mathrm{r}}} \sin(\omega_{\mathrm{r}} t) \end{pmatrix}. \tag{A4}$$

Here, we have introduced $\beta = \nu/2$ and $\omega_{\mathrm{r}} = (\omega_0^2 - \beta^2)^{1/2}$.

The same method can be used for the x direction with $\boldsymbol{x}_{\mathrm{h}}(t) = (v_{x,\mathrm{h}}(t), x_{\mathrm{h}}(t))^T$, where the shear flow is now treated as an additional (known) driving force, that is,

$$\boldsymbol{x}_{\mathrm{h}}(t) = \boldsymbol{H}(t - t_0) \boldsymbol{x}_0 + \int_{t_0}^t \boldsymbol{H}(t - t') \boldsymbol{M}(t') \boldsymbol{y}_{\mathrm{h}}(t') \, dt'. \tag{A5}$$

Here, the matrix $\boldsymbol{M}(t)$ describes the force due to the flow field,

$$\boldsymbol{M}(t) = \begin{pmatrix} 0 & \nu \dot{\gamma} \cos(\Omega t) \\ 0 & 0 \end{pmatrix}. \tag{A6}$$

Using Eq. (A3) in Eq. (A5) leads to

$$\boldsymbol{x}_{\mathrm{h}}(t) = \boldsymbol{H}(t - t_0) \boldsymbol{x}_0 + \int_{t_0}^t \boldsymbol{H}(t - t') \boldsymbol{M}(t') \boldsymbol{H}(t' - t_0) \, dt' \, \boldsymbol{y}_0. \tag{A7}$$

By carrying out the integral (computer algebra), one obtains a closed-form solution for $\boldsymbol{x}_{\mathrm{h}}(t)$ in terms of the initial conditions $\boldsymbol{x}_0$ and $\boldsymbol{y}_0$. Together with Eq. (A3), this yields all required matrix elements for $\boldsymbol{U}(t)$ in the general solution [Eq. (9)].

The explicit results are given by

$$U_{v_x v_x} = U_{v_y v_y} = e^{-\beta\theta}\left[\cos(\omega_{\mathrm{r}}\theta) - \frac{\beta}{\omega_{\mathrm{r}}}\sin(\omega_{\mathrm{r}}\theta)\right], \quad U_{xx} = U_{yy} = e^{-\beta\theta}\left[\cos(\omega_{\mathrm{r}}\theta) + \frac{\beta}{\omega_{\mathrm{r}}}\sin(\omega_{\mathrm{r}}\theta)\right],$$

$$U_{v_x x} = U_{v_y y} = -\frac{\omega_0^2}{\omega_{\mathrm{r}}}\sin(\omega_{\mathrm{r}}\theta)e^{-\beta\theta} = -\omega_0^2 U_{x v_x} = -\omega_0^2 U_{y v_y}, \quad U_{v_y v_x} = U_{v_y x} = U_{y v_x} = U_{yx} = 0,$$

$$U_{v_x v_y} = e^{-\beta\theta}\frac{4\beta\dot{\gamma}}{\Omega^2 - 4\omega_{\mathrm{r}}^2}\left\{\sin(\omega_{\mathrm{r}}\theta)\left(\frac{\Omega}{2\omega_{\mathrm{r}}}\sin(\Omega t) - \frac{2\omega_{\mathrm{r}}}{\Omega}\cos(\Omega\Theta)\sin\left[\frac{\Omega\theta}{2}\right]\right) - \cos(\omega_{\mathrm{r}}\theta)\sin(\Omega\Theta)\sin\left[\frac{\Omega\theta}{2}\right]\right.$$

$$\left. - \cos(\Omega\Theta)\frac{\beta}{\omega_{\mathrm{r}}}\left[\left(\frac{1}{2} + \frac{\omega_{\mathrm{r}}}{\Omega}\right)\sin\left(\frac{\theta(\Omega - 2\omega_{\mathrm{r}})}{2}\right) - \left(\frac{1}{2} - \frac{\omega_{\mathrm{r}}}{\Omega}\right)\sin\left(\frac{\theta(\Omega + 2\omega_{\mathrm{r}})}{2}\right)\right]\right\}, \tag{A8}$$

$$U_{xy} = e^{-\beta\theta}\frac{4\beta\dot\gamma}{\Omega^2 - 4\omega_r^2}\left\{-\sin(\omega_r\theta)\left(\frac{\Omega}{2\omega_r}\sin(\Omega t_0) + \frac{2\omega_r}{\Omega}\cos(\Omega\Theta)\sin\left[\frac{\Omega\theta}{2}\right]\right) + \cos(\omega_r\theta)\sin(\Omega\Theta)\sin\left[\frac{\Omega\theta}{2}\right]\right.$$
$$\left. + \cos(\Omega\Theta)\frac{\beta}{\omega_r}\left[\left(\frac{1}{2} + \frac{\omega_r}{\Omega}\right)\sin\left(\frac{\theta(\Omega - 2\omega_r)}{2}\right) - \left(\frac{1}{2} - \frac{\omega_r}{\Omega}\right)\sin\left(\frac{\theta(\Omega + 2\omega_r)}{2}\right)\right]\right\},$$

$$U_{xv_y} = e^{-\beta\theta}\frac{4\beta\dot\gamma/\omega_r}{\Omega^2 - 4\omega_r^2}\cos(\Omega\Theta)\left[\left(\frac{1}{2} + \frac{\omega_r}{\Omega}\right)\sin\left(\frac{\theta(\Omega - 2\omega_r)}{2}\right) - \left(\frac{1}{2} - \frac{\omega_r}{\Omega}\right)\sin\left(\frac{\theta(\Omega + 2\omega_r)}{2}\right)\right],$$

$$U_{v_x y} = e^{-\beta\theta}\frac{4\beta\dot\gamma\omega_r}{\Omega^2 - 4\omega_r^2}\left\{\sin(\omega_r\theta)\cos\left(\frac{\Omega\theta}{2}\right)\left[\sin(\Omega\Theta)\left(\frac{\beta\Omega}{\omega_r^2}\right) - \cos(\Omega\Theta)\left(1 - \frac{\beta^2}{\omega_r^2}\right)\right]\right.$$
$$\left. - \cos(\omega_r\theta)\sin\left(\frac{\Omega\theta}{2}\right)\left[\cos(\Omega\Theta)\left(\frac{2\omega_0^2 - \Omega^2}{\Omega\omega_r}\right) + \sin(\Omega\Theta)\left(\frac{2\beta}{\omega_r}\right)\right]\right\}, \tag{A9}$$

where $\theta = t - t_0$ and $\Theta = (t + t_0)/2$. The corresponding expressions for $\Omega \to 0$ can be found in Ref. [31].

APPENDIX B: EXPLICIT RESULTS FOR THE SECOND MOMENTS

The oscillatory parts of the second moments, Eq. (14), can be expressed as

$$(\boldsymbol{R})_{\alpha\beta}(t) = \frac{1}{D_{\alpha\beta}}[a_{\alpha\beta}\cos(\omega_{\alpha\beta}t) + b_{\alpha\beta}\sin(\omega_{\alpha\beta}t)], \tag{B1}$$

where $(\boldsymbol{R})_{\alpha\beta}(t) = 0$ for indices concerning the y direction only. The oscillation frequencies are $\omega_{v_x v_x} = \omega_{v_x x} = \omega_{xx} = 2\Omega$ and $\omega_{v_x v_y} = \omega_{v_x y} = \omega_{v_y x} = \omega_{xy} = \Omega$. The coefficients read

$$D_{v_x v_x} = D_{v_x x} = D_{xx} = 2(\bar v^2 + \bar\Omega^2)(\bar v^2 + 4\bar\Omega^2)[4\bar v^2\bar\Omega^2 + (\bar\Omega^2 - 4)^2][\bar v^2\bar\Omega^2 + (\bar\Omega^2 - 1)^2],$$

$$D_{v_x v_y} = D_{v_x y} = D_{v_y x} = D_{xy} = (\bar v^2 + \bar\Omega^2)[4\bar v^2\bar\Omega^2 + (\bar\Omega^2 - 4)^2],$$

$$a_{v_x v_x} = \omega_0^2\,\text{Wi}[4\bar v^6\bar\Omega^4 + \bar v^4\bar\Omega^4(13\bar\Omega^2 + 6) + \bar v^2(-13\bar\Omega^8 + 31\bar\Omega^6 + 30\bar\Omega^4 - 38\bar\Omega^2 + 8) - 4\bar\Omega^2(\bar\Omega^2 - 4)(\bar\Omega^2 - 1)^3],$$

$$b_{v_x v_x} = \omega_0^2\,\text{Wi}[8\bar v^4\bar\Omega^2(\bar\Omega^2 - 1) + \bar v^2(34\bar\Omega^6 - 41\bar\Omega^4 + 4) + 8\bar\Omega^8 - 36\bar\Omega^6 + 90\bar\Omega^4 - 86\bar\Omega^2 + 24]\bar v\bar\Omega,$$

$$a_{xx} = -b_{v_x x}/\Omega = \text{Wi}[-4\bar v^6\bar\Omega^2 - \bar v^4(13\bar\Omega^4 + 20\bar\Omega^2 - 8) - \bar v^2(-13\bar\Omega^6 + 41\bar\Omega^4 + 10\bar\Omega^2 - 8) + 4\bar\Omega^2(\bar\Omega^2 - 4)(\bar\Omega^2 - 1)^2],$$

$$b_{xx} = a_{v_x x}/\Omega = \text{Wi}[\bar v^4(-8\bar\Omega^2 + 12) + \bar v^2(-34\bar\Omega^4 + 31\bar\Omega^2 + 16) - 8\bar\Omega^6 + 22\bar\Omega^4 - 38\bar\Omega^2 + 24]\bar v\bar\Omega,$$

$$a_{v_x v_y} = \omega_0^2[-2\bar v^2 + \bar\Omega^2 - 4]\bar\Omega^2, \quad b_{v_x v_y} = \omega_0^2[-3\bar\Omega^2 + 4]\bar v\bar\Omega, \quad a_{v_y x} = \omega_0[6\bar\Omega^2 - 8]\bar v, \quad b_{v_y x} = \omega_0[-4\bar v^2 + 2\bar\Omega^2 - 8]\bar\Omega,$$

$$a_{xy} = -4\bar v^2\bar\Omega^2 + 8\bar v^2 - \bar\Omega^4 + 4\bar\Omega^2, \quad b_{xy} = [4\bar v^2 + \bar\Omega^2 + 4]\bar v\bar\Omega, \quad a_{v_x y} = \omega_0[4\bar v^2\bar\Omega^2 + \bar\Omega^4 - 2\bar\Omega^2 + 8]\bar v,$$

$$b_{v_x y} = \omega_0[4\bar v^2(\bar\Omega^2 - 1) + \bar\Omega^4 - 6\bar\Omega^2 + 8]\bar\Omega. \tag{B2}$$

[1] H. Löwen, J. Phys.: Condens. Matter **13**, R415 (2001).

[2] G. E. Morfill and A. V. Ivlev, Rev. Mod. Phys. **81**, 1353 (2009).

[3] P. K. Shukla and B. Eliasson, Rev. Mod. Phys. **81**, 25 (2009).

[4] M. Bonitz, N. Horing, and P. Ludwig, eds., *Introduction to Complex Plasmas* (Springer, Berlin, 2010).

[5] A. V. Ivlev, H. Löwen, G. E. Morfill, and C. P. Royall, *Complex Plasmas and Colloidal Dispersions: Particle-Resolved Studies of Classical Liquids and Solids* (World Scientific, Singapore, 2012).

[6] V. A. Schweigert and F. M. Peeters, Phys. Rev. B **51**, 7700 (1995).

[7] M. Kong, B. Partoens, and F. M. Peeters, New J. Phys. **5**, 23 (2003).

[8] O. Arp, D. Block, A. Piel, and A. Melzer, Phys. Rev. Lett. **93**, 165004 (2004).

[9] S. W. S. Apolinario, B. Partoens, and F. M. Peeters, New J. Phys. **9**, 283 (2007).

[10] M. Bonitz, D. Block, O. Arp, V. Golubnychiy, H. Baumgartner, P. Ludwig, A. Piel, and A. Filinov, Phys. Rev. Lett. **96**, 075001 (2006).

[11] H. Baumgartner, D. Asmus, V. Golubnychiy, P. Ludwig, H. Kählert, and M. Bonitz, New J. Phys. **10**, 093019 (2008).

[12] A. Melzer, A. Schella, J. Schablinski, D. Block, and A. Piel, Phys. Rev. Lett. **108**, 225001 (2012).

[13] C. Henning, K. Fujioka, P. Ludwig, A. Piel, A. Melzer, and M. Bonitz, Phys. Rev. Lett. **101**, 045002 (2008).

[14] A. Melzer, M. Klindworth, and A. Piel, Phys. Rev. Lett. **87**, 115002 (2001).

[15] M. Klindworth, A. Melzer, A. Piel, and V. A. Schweigert, Phys. Rev. B **61**, 8404 (2000).

[16] M. Rex and H. Löwen, Phys. Rev. Lett. **101**, 148302 (2008).

[17] Z. T. Németh and H. Löwen, J. Phys.: Condens. Matter **10**, 6189 (1998).

[18] Z. T. Németh and H. Löwen, Phys. Rev. E **59**, 6824 (1999).

[19] W. K. Kegel, J. Chem. Phys. **115**, 6538 (2001).

[20] G. L. Hunter and E. R. Weeks, Rep. Prog. Phys. **75**, 066501 (2012).

[21] R. Bubeck, C. Bechinger, S. Neser, and P. Leiderer, Phys. Rev. Lett. **82**, 3364 (1999).

[22] J. Carstensen, F. Greiner, L.-J. Hou, H. Maurer, and A. Piel, Phys. Plasmas **16**, 013702 (2009).

[23] J. Carstensen, F. Greiner, and A. Piel, Phys. Plasmas **17**, 083703 (2010).

[24] H. Kählert, J. Carstensen, M. Bonitz, H. Löwen, F. Greiner, and A. Piel, Phys. Rev. Lett. (to appear).

[25] P. Schall and M. van Hecke, Annu. Rev. Fluid Mech. **42**, 67 (2010).

[26] J. Dhont, *An Introduction to Dynamics of Colloids* (Elsevier Science, Amsterdam, 1996).

[27] D. Derks, H. Wisman, A. van Blaaderen, and A. Imhof, J. Phys. Condens. Matter **16**, 3917 (2004).

[28] R. Besseling, L. Isa, E. R. Weeks, and W. C. K. Poon, Adv. Colloid Interfac. **146**, 1 (2009).

[29] L. T. Shereda, R. G. Larson, and M. J. Solomon, Phys. Rev. Lett. **105**, 228302 (2010).

[30] G. Guidarelli, F. Craciun, C. Galassi, and E. Roncari, Ultrasonics **36**, 467 (1998).

[31] R. Rzehak and W. Zimmermann, Phys. A (Amsterdam, Neth.) **324**, 495 (2003).

[32] J. Bammert and W. Zimmermann, Phys. Rev. E **82**, 052102 (2010).

[33] L. Holzer, J. Bammert, R. Rzehak, and W. Zimmermann, Phys. Rev. E **81**, 041124 (2010).

[34] B. Lander, U. Seifert, and T. Speck, Phys. Rev. E **85**, 021103 (2012).

[35] A. Ziehl, J. Bammert, L. Holzer, C. Wagner, and W. Zimmermann, Phys. Rev. Lett. **103**, 230602 (2009).

[36] J.-C. Meiners and S. R. Quake, Phys. Rev. Lett. **82**, 2211 (1999).

[37] M. Radu and T. Schilling, arXiv:1203.3441.

[38] C. van den Broeck, J. M. Sancho, and M. San Miguel, Phys. A (Amsterdam, Neth.) **116**, 448 (1982).

[39] R. Mauri and D. Leporini, Europhys. Lett. **76**, 1022 (2006).

[40] P. P. J. M. Schram and S. A. Trigger, Phys. B (Amsterdam, Neth.) **228**, 91 (1996).

[41] G. Da Prato and A. Lunardi, J. Evol. Equ. **7**, 587 (2007).

[42] F. Knäble, J. Evol. Equ. **11**, 959 (2011).

[43] E. Coddington and R. Carlson, *Linear Ordinary Differential Equations* (Society for Industrial and Applied Mathematics, Philadelphia, 1997).

[44] W. Coffey, Y. Kalmykov, and J. Waldron, *The Langevin Equation: With Applications to Stochastic Problems in Physics, Chemistry, and Electrical Engineering* (World Scientific, Singapore, 2004).

[45] R. Mannella, Phys. Rev. E **69**, 041107 (2004).

[46] S. G. Amiranashvili, N. G. Gousein-zade, and V. N. Tsytovich, Phys. Rev. E **64**, 016407 (2001).

[47] C. Henning, H. Kählert, P. Ludwig, A. Melzer, and M. Bonitz, J. Phys. A: Math. Theor. **42**, 214023 (2009).

[48] L. Gammaitoni, P. Hänggi, P. Jung, and F. Marchesoni, Rev. Mod. Phys. **70**, 223 (1998).

[49] P. Romanczuk, M. Bär, W. Ebeling, B. Lindner, and L. Schimansky-Geier, Eur. Phys. J.-Spec. Top. **202**, 1 (2012).

[50] J. Dunkel, W. Ebeling, and S. A. Trigger, Phys. Rev. E **70**, 046406 (2004).